Available online at www.sciencedirect.com
ScienceDirect
Journal of Molecular Catalysis A: Chemical 275 (2007) 183–193
JOURNAL OF MOLECULAR CATALYSIS A: CHEMICAL
www.elsevier.com/locate/molcata

Dehydration of methanol to dimethyl ether over Nb_2O_5 and $NbOPO_4$ catalysts: Microcalorimetric and FT-IR studies

Qing Sun [a,b], Yuchuan Fu [a], Haixia Yang [a], Aline Auroux [b,*], Jianyi Shen [a,**]

[a] *Lab of Mesoscopic Chemistry, School of Chemistry and Chemical Engineering, Nanjing University, Nanjing 210093, China*
[b] *Institut de Recherches sur la Catalyse et l'Environnement de Lyon, UMR 5256, CNRS-Université Lyon 1, 2 Avenue Albert Einstein, 69626 Villeurbanne Cedex, France*

Received 15 May 2007; accepted 11 June 2007
Available online 16 June 2007

Abstract

The unique properties of Nb_2O_5 as a solid acid have led to catalytic applications in various reactions catalyzed by acids. The surface acidity and stability of Nb_2O_5 can be enhanced by the addition of phosphate ions. In this work, amorphous Nb_2O_5 and $NbOPO_4$ samples were synthesized. The interactions of ammonia, methanol, water and dimethyl ether with Nb_2O_5 and $NbOPO_4$ were investigated by means of adsorption microcalorimetry, adsorption infrared spectroscopy (FT-IR) and temperature-programmed desorption (TPD) techniques. The results of microcalorimetry and FT-IR for NH_3 adsorption have shown that $NbOPO_4$ is much more acidic than Nb_2O_5 due to its higher surface area, and that both Brønsted and Lewis acid sites are present on the surface of Nb_2O_5 and $NbOPO_4$. Water adsorption microcalorimetry results indicate that a small amount of water was strongly chemisorbed on Nb_2O_5 and $NbOPO_4$ while most of the adsorbed water corresponded to physical adsorption. The results of methanol adsorption microcalorimetry, methanol adsorption FT-IR and methanol TPD suggest that methanol is mainly strongly dissociatively adsorbed on Nb_2O_5 and $NbOPO_4$ to form methoxy species and DME could be produced from the dehydration of methoxy species. DME adsorption microcalorimetry and FT-IR showed that DME was mainly molecularly chemically adsorbed on Nb_2O_5 and $NbOPO_4$, while a small amount of DME was dissociatively adsorbed. The probe molecules (NH_3, methanol, H_2O and DME) used in this work were adsorbed more strongly on $NbOPO_4$ than on Nb_2O_5 because of the stronger acidity of $NbOPO_4$. In the reaction of methanol dehydration, although Nb_2O_5 and $NbOPO_4$ were not as active as a H-ZSM-5 zeolite, they exhibited 100% selectivity to the DME product and a good stability of the activity in the temperature range relevant to the reaction (453–573 K), without coke formation.

Keywords: Nb_2O_5; Niobium phosphate; Methanol; DME; Adsorption microcalorimetry; Acidity

1. Introduction

Dimethyl ether (DME) has been widely used as an aerosol propellant to replace chlorofluoro carbons [1]. Additionally, it is an important chemical intermediate for producing many valuable chemicals such as lower olefins, methyl acetate, dimethyl sulfate, . . . [2,3]. In recent years, it has attracted global attention as a potential clean fuel substitute for LPG and diesel oil, due to its cleanness, non-toxicity and environmentally benign behavior [4,5].

DME can be synthesized by dehydration of methanol over solid acidic catalysts [6–9]. It can also be synthesized directly from syngas via a so-called STD (syngas to DME) process by employing a hybrid catalyst comprising a methanol synthesis component and a solid acid [10,11], which is more attractive in consideration of the equilibrium limitation. Typically, a $Cu/ZnO/Al_2O_3$ catalyst is used as the methanol synthesis component in the hybrid catalyst [11,12], and the solid acids used for the dehydration of methanol are H-ZSM-5, H-Y zeolites, γ-Al_2O_3, modified γ-Al_2O_3, silica-alumina, etc. [8,9,11,13,14].

Among the solid acids used for methanol dehydration, H-ZSM-5 and γ-Al_2O_3 are the two catalysts that have been studied intensively both for academic and commercial purposes [6,12,15]. H-ZSM-5 has been reported to be an effective methanol dehydration catalyst, but on which hydrocarbon byproducts are generated, thus leading to a decrease of the activ-

* Corresponding author.
** Corresponding author.
E-mail addresses: aline.auroux@ircelyon.univ-lyon1.fr (A. Auroux), jyshen@nju.edu.cn (J. Shen).

1381-1169/$ – see front matter © 2007 Elsevier B.V. All rights reserved.
doi:10.1016/j.molcata.2007.06.008

ity [7,11,15]. This is due to the strong acidity of the H-ZSM-5, which catalyzes the conversion of methanol to hydrocarbons and even coke [11,15]. Although the DME selectivity is high for methanol dehydration on γ-Al_2O_3 [7,15], it exhibits much lower activity than H-ZSM-5 [7,11,15].

Niobium pentoxide (Nb_2O_5) is a white solid, stable in air and insoluble in water. Hydrated niobium oxide ($Nb_2O_5{\cdot}nH_2O$) exhibits strong acidity according to the Hammett titration ($H_0 \leq -5.6$). Its acid strength is equivalent to about 70% sulfuric acid [16]. It possesses both Lewis and Brønsted acid sites [17]. It usually exhibits high activity for the acid-catalyzed reactions in which water molecules participate [16,18]. Niobium phosphate ($NbOPO_4$) has a similar structure to Nb_2O_5 [19], but with a higher acid strength ($H_0 \leq -8.2$). Terminal P–OH and Nb–OH groups co-exist at the surface of bulk and impregnated niobium phosphate catalysts [20]. On these materials, the P–OH groups are stronger Brønsted acids than Nb–OH [21]. The Lewis acid sites in niobium phosphate catalysts are the coordinatively unsaturated Nb^{5+} cations [21].

Okazaki et al. have reported that the activity of niobium oxide for the reaction of methanol dehydration to DME could be enhanced by the addition of H_3PO_4 on Nb_2O_5 [22].

In this work, amorphous Nb_2O_5 and $NbOPO_4$ samples were prepared. Adsorption microcalorimetry experiments using different gases (NH_3, methanol, water and DME) as probe molecules were carried out to determine the number and strength of the active sites on Nb_2O_5 and $NbOPO_4$, and adsorption FT-IR and TPD techniques were used to determine the nature of the adsorbed surface species. The catalytic activities of Nb_2O_5 and $NbOPO_4$ were evaluated in the reaction of methanol dehydration to DME.

2. Experimental

2.1. Catalyst preparation

Nb_2O_5 was prepared by calcining commercial niobic acid ($Nb_2O_5{\cdot}nH_2O$, CBMM, Brazil) at 623 K for 4 h in air flow. A porous niobium phosphate, denoted as $NbOPO_4$, was prepared by following a previously described procedure [23]. Specifically, 2.73 g of $NbCl_5$ (Alfa Aesar, 99%) was partially hydrolyzed in 50 ml H_2O, and 2.30 g H_3PO_4 (Aldrich, 85% aqueous solution) was added, upon which a vigorous hydrolytic reaction occurred. An additional 50 ml H_2O was then added and the reaction mixture was stirred for 30 min, after which an aqueous solution of ammonia (25%) was added to adjust the pH of the reaction mixture to 2.60. After stirring for a few minutes, the slurry was filtered and washed with deionized water to obtain a chlorideless gel. The gel was mixed with 10 ml H_2O and 1.45 g hexadecylamine (Aldrich, 90%) and stirred for 30 min. Then, 0.92 g H_3PO_4 (85%) was added and the pH of the mixture was adjusted to 3.9. After stirring for 30 min, the gel was heated in a Teflon lined stainless steel autoclave at 338 K under autogenous pressure for 2 days. The final product was filtered, washed with deionized water, dried at 373 K overnight and calcined at 625 K in N_2 for 12 h, then in air up to 723 K for 40 h.

2.2. Catalyst characterization

The X-ray diffraction (XRD) measurements were carried out on a Bruker D5005 diffractometer scanning from 3° to 80° (2θ) at a rate of 0.02° s^{-1} using a Cu Kα radiation (λ = 0.15418 nm) source. The applied voltage and current were 50 kV and 35 mA, respectively. The surface area and pore size were measured by nitrogen adsorption at 77 K after heat pretreatment under vacuum at 673 K for 4 h. Elemental analysis was performed using ICP atomic emission spectroscopy (Spectroflame-ICP D, Spectro). The X-ray photoelectron spectra (XPS) were measured on a SSI 301 instrument equipped with a hemispherical electron analyzer and an Al anode (Al Kα = 1486.6 eV) powered at 100 W. The residual pressure in the spectrometer chamber was 5×10^{-8} Pa during data acquisition.

The microcalorimetric studies of methanol, water and DME adsorption were performed at 303 K, while ammonia adsorption was performed at 423 K, in a heat flow calorimeter (C80 from Setaram) linked to a conventional volumetric apparatus equipped with a Barocel capacitance manometer for pressure measurements. All the gases used for measurements (purity > 99.9%) were purified by successive freeze–pump–thaw cycles. Before any adsorption, about 100 mg of sample was pretreated in a quartz calorimetric cell under evacuation overnight at 623 K. The differential heats of adsorption were measured as a function of coverage by repeatedly introducing small doses of gas or vapor onto the catalyst until an equilibrium pressure of about 66 Pa was reached [24]. The sample was then outgassed for 30 min at the same temperature and a second adsorption was performed at the same temperature until an equilibrium pressure of about 27 Pa was attained; this made it possible to calculate the irreversibly chemisorbed amount of probe molecule at this pressure.

Temperature-programmed desorption of water (or methanol) was performed on a Setaram TG-DSC 111 equipment coupled with a mass spectrometer (Thermostar from Pfeifer) as a detector. A capillary-coupling system was used. The TPD experiments were carried out in a flow, with helium as the carrier gas (10 ml min^{-1}). For each experiment, about 30 mg of a sample containing water (or methanol) absorbed in a previously performed microcalorimetric experiment was used. The sample was heated at 5 K min^{-1} in helium up to 873 K. During this temperature increase, the gas phase composition was analyzed by mass spectrometry.

The gas adsorption FT-IR spectra were recorded with a Bruker Vector 22 FT-IR spectrophotometer (DTGS detector) in the 4000–400 cm^{-1} range, with a resolution of 2 cm^{-1} and 50 acquisition scans. The self-supporting wafer (10–30 mg, 18 mm diameter) was first activated in an in situ IR cell at 673 K in O_2 flow for 12 h, evacuated at the same temperature for 2 h, and then exposed to the different gases (NH_3, methanol and dimethyl ether) (purity > 99.9%) at room temperature for 5 min. The desorption was carried out by evacuation for 30 min each at 300, 373, 473, 523, 573 and 673 K, respectively. A spectrum was recorded at room temperature after desorption at each temperature.

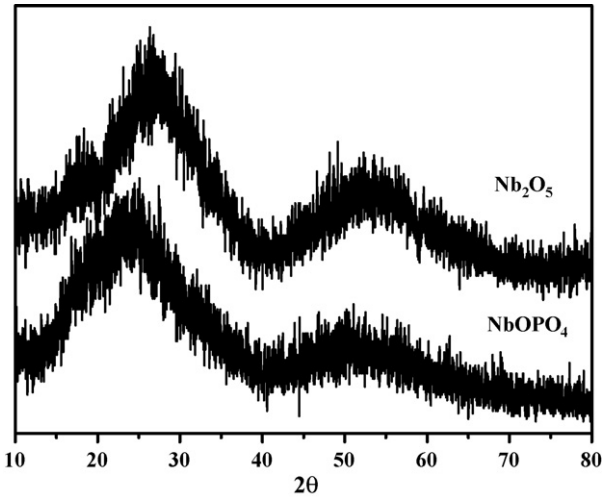

Fig. 1. XRD pattern of Nb_2O_5 and $NbOPO_4$ catalysts.

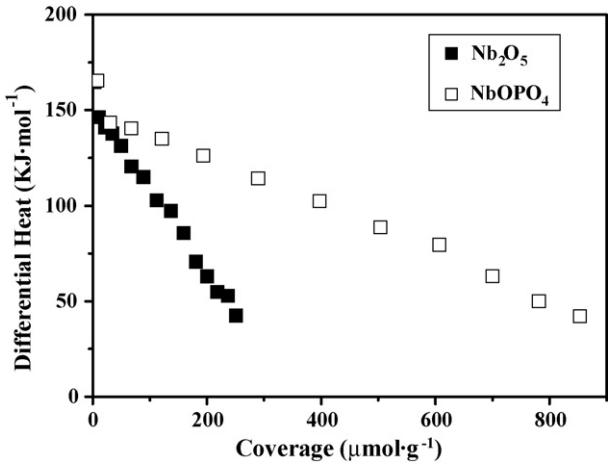

Fig. 2. Differential heat vs. coverage (per g of catalyst) for NH_3 adsorption at 423 K over Nb_2O_5 and $NbOPO_4$ catalysts.

2.3. Catalytic reaction

The dehydration of methanol was carried out in a fixed microreactor made of stainless steel with an inner diameter of 6 mm. Methanol was introduced into the reaction zone by bubbling N_2 (99.999%) through a glass saturator filled with methanol (AR) maintained at 303 K. In each test, 0.2 g catalyst was loaded, and the gas hourly space velocity (GHSV) was 3400 ml g^{-1} h^{-1}. The feed composition was maintained at methanol:N_2 = 21:79. The tail gas out of the reactor was analyzed 30 min after reaching the reaction temperature by an on-line GC equipped with an FID detector. The column used was PEG 20M for the separation of methanol, DME and other organic compounds. The gas lines were kept at 383 K to prevent condensation of the reactant and products. The reaction was carried out at atmospheric pressure.

3. Results and discussions

3.1. Structural characterizations

The XRD results shown in Fig. 1 indicate that the Nb_2O_5 and $NbOPO_4$ samples studied in this work were amorphous. They mainly exhibited two broad 2θ peaks around 25° and 52°. The peaks were shifted to lower angles for $NbOPO_4$, implying some difference in bonding in $NbOPO_4$ compared to Nb_2O_5.

Results of bulk and surface elemental analysis, as well as the surface area and porosity data for the samples, are given in Table 1. $NbOPO_4$ presented a much higher surface area (511 m^2 g^{-1}) than Nb_2O_5 (110 m^2 g^{-1}), since $NbOPO_4$ was prepared by using a template. The pore diameter of $NbOPO_4$ (4.4 nm) was slightly smaller than that of Nb_2O_5 (6.0 nm), but the pore volume of $NbOPO_4$ (0.56 ml g^{-1}) was much larger than for Nb_2O_5 (0.16 ml g^{-1}). The chemical analysis showed a Nb/P atomic ratio of 1:1 in $NbOPO_4$. XPS results showed that P might be in slight excess on the surface (see Table 1).

Previous data had already shown the non-oxidative properties of Nb_2O_5 and $NbOPO_4$, evidenced by the absence of any hydrogen consumption peaks until 1100 K in temperature-programmed reduction experiments [25].

3.2. Adsorption microcalorimetry

The surface acidity in terms of number of acid sites and site strengths was determined by ammonia adsorption microcalorimetry, and the results are presented in Fig. 2. Methanol, water and DME adsorption microcalorimetry measurements were carried out to determine the number, strength and strength distribution of the surface sites on Nb_2O_5 and $NbOPO_4$ and the results are shown in Figs. 3–6. Table 2 summarizes quantitative results for the initial heats of adsorption, irreversibly adsorbed volumes and total adsorbed volumes probed by different molecules (ammonia, methanol, water and DME) per square meter of surface (μmol m^{-2}) and per gram of sample (μmol g^{-1}) under an equilibrium pressure of 27 Pa.

3.2.1. NH_3 adsorption microcalorimetry

Nb_2O_5 can be regarded as a strong acid according to Hammett titration [16]. It has been shown that its surface acidity

Table 1
Chemical analysis, X-ray photoelectronic spectroscopy analysis, BET surface area, average pore radius, and pore volume of the samples

Sample	C.A. (wt%)		XPS (wt%)		BET (m^2 g^{-1})	Average pore diameter (nm)	Pore volume (ml g^{-1})
	Nb	P	Nb	P			
Nb_2O_5	–	–	–	–	110	6.0	0.16
$NbOPO_4$	42.6	12.4	12.1	12.7	511	4.4	0.56

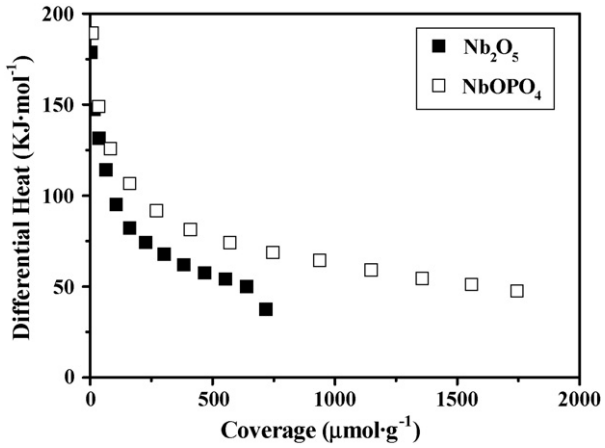

Fig. 3. Differential heat vs. coverage (per g of catalyst) for H_2O adsorption at 303 K over Nb_2O_5 and $NbOPO_4$ catalysts.

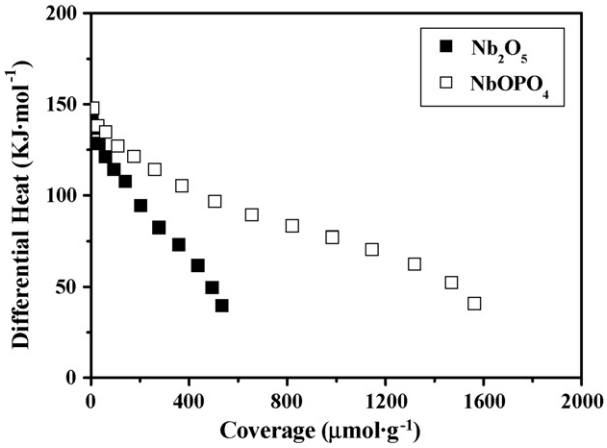

Fig. 5. Differential heat vs. coverage (per g of catalyst) for methanol adsorption at 303 K over Nb_2O_5 and $NbOPO_4$ catalysts.

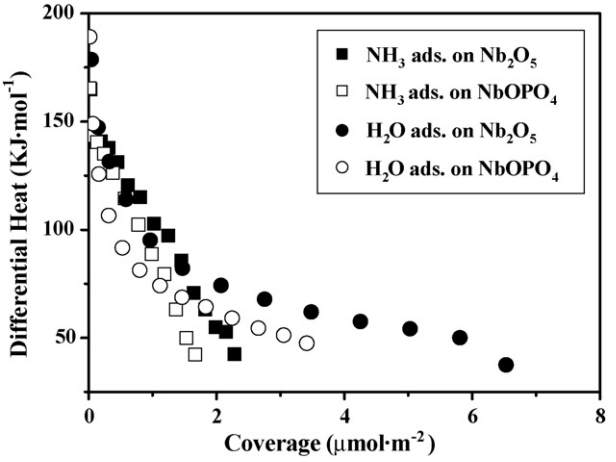

Fig. 4. Differential heat vs. coverage (per square meter of catalyst) for NH_3 adsorption at 423 K and H_2O adsorption at 303 K over Nb_2O_5 and $NbOPO_4$ catalysts.

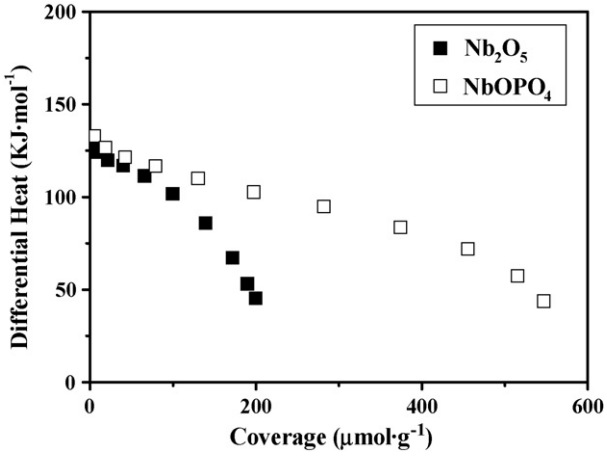

Fig. 6. Differential heat vs. coverage (per g of catalyst) for DME adsorption at 303 K over Nb_2O_5 and $NbOPO_4$ catalysts.

Table 2
Number and strength of acid sites as determined by adsorption microcalorimetry under an equilibrium pressure of 27 Pa at 423 K

Sample	Probe	V_{tot}[a] (27 Pa) (μmol g^{-1})	V_{tot}[a] (27 Pa) (μmol m^{-2})	V_{irr}[b] (27 Pa) (μmol g^{-1})	V_{irr}[b] (27 Pa) (μmol m^{-2})	Q_{init}[c] (kJ mol^{-1})	Q_{int}[d] (27 Pa) (J g^{-1})
Nb_2O_5	NH_3	208	1.9	89	0.8	165	22.4
$NbOPO_4$		716	1.4	298	0.6	165	76.5
Nb_2O_5	CH_3OH	483	4.4	341	3.1	142	44.0
$NbOPO_4$		1365	2.7	977	1.9	148	126.1
Nb_2O_5	DME	184	1.7	117	1.1	130	18.5
$NbOPO_4$		499	1.0	300	0.6	133	48.6
Nb_2O_5	H_2O	526	4.8	166	1.5	179	42.0
$NbOPO_4$		1260	2.5	411	0.8	189	101.2

[a] Total amount of NH_3, methanol, DME and water retained as determined at 27 Pa of equilibrium pressure.
[b] "Irreversible" amount of NH_3, methanol, DME and water retained as determined from the difference between the amounts adsorbed in the first and second adsorptions at 27 Pa, which represents the amount of strong sites.
[c] Heat evolved from the first NH_3, methanol, DME and water dose.
[d] Integral heat evolved at 27 Pa of NH_3, methanol, DME and water equilibrium pressure.

can be enhanced and stabilized via addition of phosphate ions [19]. In this work, the initial heat and saturation coverage for ammonia adsorption on Nb_2O_5 were found to be about 165 kJ mol^{-1} and 250 μmol g^{-1}, respectively (see Fig. 2). The initial heat did not vary with the addition of PO_4^{3-} into Nb_2O_5, However, the saturation coverage of NH_3 on $NbOPO_4$ was found to be about 850 μmol g^{-1}, much higher than for Nb_2O_5, which is apparently due to the high surface area of $NbOPO_4$. In fact, when the surface coverage is expressed in terms of the amount of ammonia adsorbed on a unit surface area, the coverage on $NbOPO_4$ was lower than Nb_2O_5 (see Fig. 4 and Table 2).

3.2.2. H_2O adsorption microcalorimetry

Polar molecules with different gas phase affinities such as alcohol and water are usually used to measure the hydrophilic and hydrophobic properties of the surface of materials [26–30]. The differential heat and saturation coverage reflect the proton affinity and the strength of H-bonds or van der Waals forces on those samples.

The results of H_2O adsorption in terms of number and strength of adsorption sites on Nb_2O_5 and $NbOPO_4$ are shown in Fig. 3. The initial heats for H_2O adsorption on Nb_2O_5 and $NbOPO_4$ were very high, 179 and 189 kJ mol^{-1}, respectively. With the increase of H_2O coverage, the differential heats first dropped sharply and then decreased gradually until the saturation coverage was reached at 67 Pa of equilibrium pressure (763 μmol g^{-1} for Nb_2O_5 and 1800 μmol g^{-1} for $NbOPO_4$). For example, on Nb_2O_5, the differential heat of H_2O adsorption first decreased dramatically to around 80 kJ mol^{-1}, for a H_2O coverage of 1.5 μmol m^{-2} (see Fig. 4), then it decreased slowly until it reached a value close to the latent heat of liquefaction of water (44 kJ mol^{-1}). Bolis et al. have suggested that the high differential heat values (Q_{diff} > 100 kJ mol^{-1}) observed at low coverage are compatible with the energy of coordination of H_2O on Lewis acid sites, while adsorbed water on a Brønsted site acts as an H-bond acceptor of the Brønsted acidic proton with a differential heat of the order of 70 kJ mol^{-1} [31]. Therefore, in this work, H_2O might be adsorbed first on the small amount of coordinatively unsaturated Nb^{5+} cations which act as Lewis acid sites, and then on Brønsted sites or on strongly polarized H_2O molecules already adsorbed on Lewis sites, as suggested in the literature [31].

The differential heats versus coverage per square meter for NH_3 adsorption and H_2O adsorption on Nb_2O_5 and $NbOPO_4$ are compared in Fig. 4. It can be seen that for both NH_3 and H_2O adsorption, the coverage per square meter of surface was higher on Nb_2O_5 than on $NbOPO_4$. Moreover, the coverage for water adsorption was much higher than for ammonia adsorption, which suggests a larger amount of physically adsorbed H_2O on Nb_2O_5 and $NbOPO_4$. It has been reported in the literature that the initial heats for water adsorption are 60 kJ mol^{-1} on silica [27], 160 kJ mol^{-1} on H-BEA zeolites [31] and 100 kJ mol^{-1} on H-ZSM-5 [32]. Thus, the Nb_2O_5 and $NbOPO_4$ samples studied in this work were quite hydrophilic and exhibited high strength of H-bonding, $NbOPO_4$ more so than Nb_2O_5.

3.2.3. Methanol adsorption microcalorimetry

Fig. 5 shows the results of methanol adsorption on Nb_2O_5 and $NbOPO_4$. The initial heats of adsorption and saturation coverage were found to be about 142 kJ mol^{-1} and 533 μmol g^{-1} on Nb_2O_5, respectively, while $NbOPO_4$ exhibited a slightly higher initial heat of 148 kJ mol^{-1} and a much higher methanol coverage of 1563 μmol g^{-1} due to its large surface area. However, the methanol coverage in terms of the amount per unit surface area on $NbOPO_4$ was lower than on Nb_2O_5, in agreement with what was observed for NH_3 adsorption (see Table 2). Both Nb_2O_5 and $NbOPO_4$ strongly interact with methanol as indicated by the differential heats, which are higher than those on silica (Q_{init} = 60 to 90 kJ mol^{-1}) [26,28,32–34] and H-ZSM-5 (Q_{init} = 115 kJ mol^{-1}) [32] but lower than on γ-Al_2O_3 (Q_{init} > 200 kJ mol^{-1}) [35].

It has been reported in the literature that there exist different methanol adsorption heat steps on silica [34] and on γ-Al_2O_3 [35] at low and high coverage, indicating different methanol adsorption modes on them. Adsorption occurring at low coverage might be strong chemical adsorption, while adsorption at high coverage corresponds to physical adsorption in which hydrogen bonding plays an important role [35]. However, in the present work, the differential heats of methanol adsorption on Nb_2O_5 and $NbOPO_4$ decreased monotonically with increasing methanol coverage, and there was no apparent plateau observed in methanol adsorption heats. Note that outgassing at 673 K overnight (the pretreatment conditions used in this study) might remove more weak surface hydroxyl groups compared to the pretreatment conditions used in the literature (outgassing at 600 K for 2 h) [34]. Therefore, only quite strong acid sites remained and methanol adsorbed strongly on them.

In addition, by comparing the total adsorbed methanol volume (V_{tot}) with the irreversibly adsorbed volume (V_{irr}) (see Table 2), it is clearly shown that most of adsorbed methanol was strongly chemisorbed on Nb_2O_5 and $NbOPO_4$. Moreover, both the total adsorbed methanol volume (V_{tot}) and the irreversibly adsorbed volume (V_{irr}) were much larger than those for NH_3 adsorption which titrates the surface acid sites. For example, on Nb_2O_5, the total adsorbed methanol volume (V_{tot}) and the irreversibly adsorbed volume (V_{irr}) were 483 and 341 μmol g^{-1}, respectively, while those for NH_3 adsorption were only 208 and 89 μmol g^{-1}. This might suggest that methanol was mainly dissociatively adsorbed on Nb_2O_5 and $NbOPO_4$, since the water formed by the dissociative adsorption of methanol might hydrate the surface of Nb_2O_5 and $NbOPO_4$, thereby generating new hydroxyl groups favoring further methanol adsorption.

3.2.4. DME adsorption microcalorimetry

DME was also used as a basic molecule to probe the surface acidity on the catalyst. The bridged oxygen in the DME molecule has unshared pairs of electrons and can act as electron donor.

Very few articles in the literature discuss DME adsorption microcalorimetry. It has been reported that DME is a better probe molecule than NH_3 in adsorption microcalorimetry for studying the acidity of sulfated metal oxides [36]. It is believed that the

difference between NH_3 and DME adsorption is probably due to the different polarizabilities of these two probe molecules [37]. The basicity and polarizability of DME are more similar to those of light paraffins than to NH_3. So, DME could provide a more specific way to distinguish the interactions of solid acids with paraffins [37].

In this work, as depicted in Fig. 6, the initial heats for DME adsorption on Nb_2O_5 and $NbOPO_4$ were 130 and 133 kJ mol^{-1}, respectively. The corresponding saturation coverages for DME adsorption on Nb_2O_5 and $NbOPO_4$ were 200 and 547 μmol m^{-1} at an equilibrium pressure of 67 Pa, respectively. Measurements of the initial heats of DME adsorption on zirconium sulfate and iron sulfate have been reported in the literature, with values of 140 and 105 kJ mol^{-1}, respectively [36]. This suggests that the acidities of Nb_2O_5 and $NbOPO_4$ are stronger than that of iron sulfate but weaker than that of zirconium sulfate. It should be noted that the irreversible adsorption volumes (see Table 2) for DME adsorption on Nb_2O_5 (117 μmol g^{-1}) and $NbOPO_4$ (300 μmol g^{-1}) were close to those for NH_3 adsorption (89 μmol g^{-1} for Nb_2O_5 and 298 μmol g^{-1} for $NbOPO_4$), which might suggest that one DME molecule is adsorbed on each acid site.

3.3. Temperature-programmed desorption

3.3.1. Water-TPD

Fig. 7 shows the H_2O-TPD results for the Nb_2O_5 and $NbOPO_4$ samples. Both of them exhibited a broad desorption peak which revealed the heterogeneous strength distribution of the adsorption sites on them, in agreement with the results of H_2O adsorption. It is usually not accurate to rank the sites strengths by simply comparing the desorption maxima because of complex diffusion effects, especially for porous materials. The temperatures of peak maxima were slightly higher for $NbOPO_4$ than for Nb_2O_5. In addition, the areas of the desorption peaks reflected the relative populations of adsorption sites, which clearly show that $NbOPO_4$ possessed much more adsorption sites than Nb_2O_5, in good agreement with the microcalorimetric adsorption results.

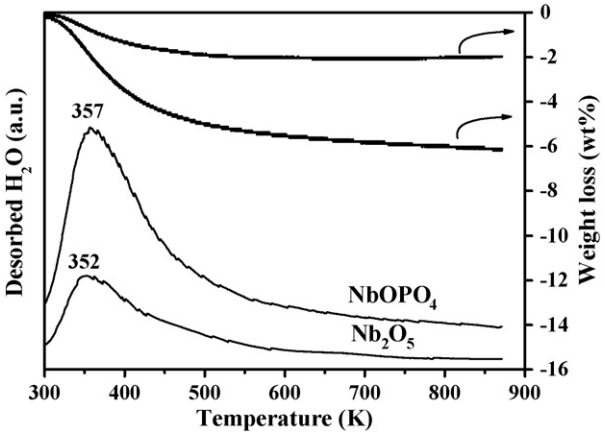

Fig. 7. Temperature-programmed desorption (TPD) profiles of adsorbed H_2O on Nb_2O_5 and $NbOPO_4$ catalysts as studied by TG–MS.

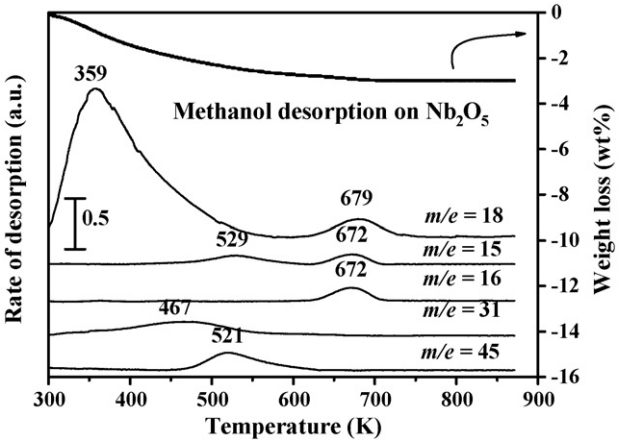

Fig. 8. Temperature-programmed desorption (TPD) profiles of adsorbed methanol on Nb_2O_5 (*m/e*: methanol 31, water 18, dimethyl ether 45, methane 15 and 16).

3.3.2. Methanol TPD

The methanol TPD results for Nb_2O_5 and $NbOPO_4$ are shown in Figs. 8 and 9, respectively. Both Nb_2O_5 and $NbOPO_4$ desorbed large amounts of water (*m/e* = 18) which might have been formed by methanol condensation on the surface of Nb_2O_5 and $NbOPO_4$. However, the possibility of the samples adsorbing some water in air during the transfer from one apparatus to the other could not be excluded. This suggested again the strong hydrophilic properties of Nb_2O_5 and $NbOPO_4$.

Fig. 8 shows that methanol (*m/e* = 31) adsorbed on Nb_2O_5 was released with a broad peak maximum around 470 K, followed by DME (*m/e* = 45), methane (*m/e* = 16, 15), and additional H_2O (*m/e* = 18) desorptions at 521, 672 and 679 K, respectively. The weak peak appearing around 529 K for the *m/e* = 15 signal is due to the second fragmentation of DME in mass detection. From the relative intensities of the peaks, we might propose that a small amount of the adsorbed methanol is weakly bonded to Nb_2O_5, while most of the methanol interacts with Nb_2O_5 leading to the formation of methoxy groups (as seen by FT-IR). These surface methoxy groups further formed

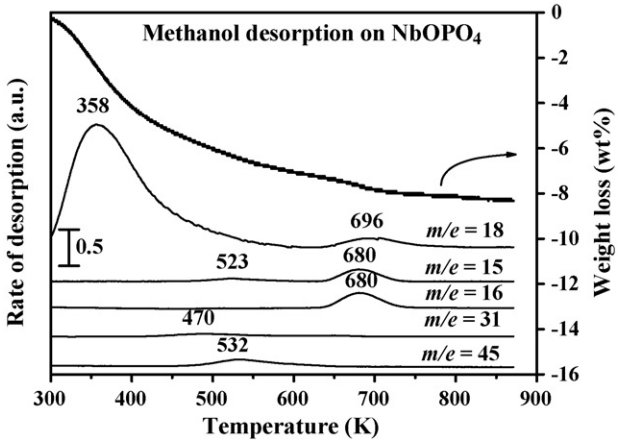

Fig. 9. Temperature-programmed desorption (TPD) profiles of adsorbed methanol on $NbOPO_4$ (*m/e*: methanol 31, water 18, dimethyl ether 45, methane 15 and 16).

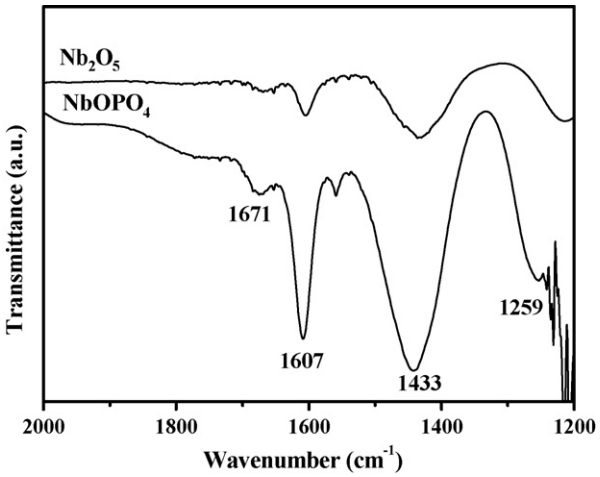

Fig. 10. FT-IR spectra after NH_3 adsorption and desorption at 300 K on Nb_2O_5 and $NbOPO_4$ catalysts.

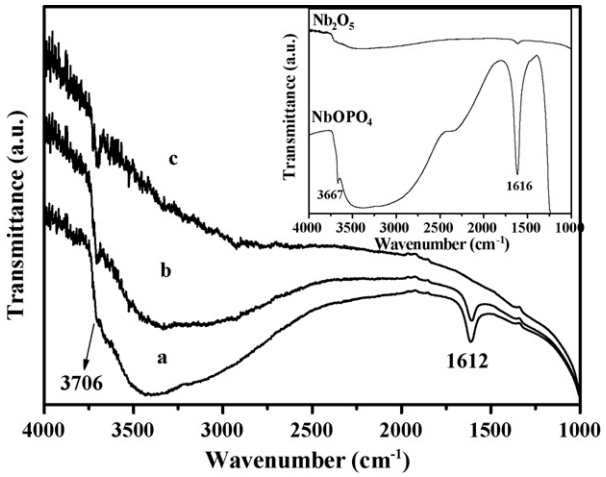

Fig. 11. FT-IR absorption bands of OH groups of the Nb_2O_5 desorbed at different temperatures: (a) 300 K, (b) 423 K, (c) 573 K (*inset*: FT-IR absorption bands of OH groups of the Nb_2O_5 and $NbOPO_4$ desorbed at 300 K).

DME with the increase of temperature, which is in good agreement with the results in the literature. It is interesting to observe that some methoxy species are very stable as they decompose to methane and H_2O at only 672 K. The desorption profile for $NbOPO_4$ displayed similar features, but the intensities of the peaks were much higher than for Nb_2O_5, as shown in Fig. 9. Additionally, the desorption peaks due to DME and methane both appeared at higher temperatures (532 and 680 K) than on Nb_2O_5, which suggests a better stability of methoxy species on $NbOPO_4$ than on Nb_2O_5. Note that we did not observe any signal due to CO ($m/e = 28$) and CO_2 ($m/e = 44$), suggesting the lack of oxidative properties of Nb_2O_5 and $NbOPO_4$.

3.4. Adsorption FT-IR

3.4.1. NH_3 adsorption FT-IR

Fig. 10 shows the FT-IR spectra of Nb_2O_5 and $NbOPO_4$ after NH_3 adsorption and desorption at 300 K. Both Brønsted and Lewis acid sites were present on the samples. The bands around 1671 and 1433 cm^{-1} are due to the deformation vibration of NH_4^+ formed by the interaction of NH_3 with Brønsted acid sites, while the bands at 1607 and 1259 cm^{-1} originate from the asymmetric and symmetric deformation vibrations, respectively, for NH_3 coordinated to Nb^{5+}. Apparently, $NbOPO_4$ exhibited higher surface B and L acidities than Nb_2O_5, according to the relative intensities of the peaks around 1433 and 1607 cm^{-1}, respectively.

3.4.2. OH groups

The FT-IR spectra of the Nb_2O_5 and $NbOPO_4$ samples after outgassing from 300 up to 773 K are reported in Figs. 11 and 12. In Fig. 11, the spectrum of Nb_2O_5 after outgassing at 300 K shows a sharp peak at 3706 cm^{-1} and a broad absorption band centered near 3400 cm^{-1}, which are assigned to the OH stretching mode of free Nb–OH groups and H-bonded hydroxyl groups [21]. The analysis of the lower frequency region showed a band present at 1612 cm^{-1}, due to the scissoring mode of adsorbed molecular water. Outgassing at 423 K caused a decrease of the broad absorption band around 3400 cm^{-1}, a notable reduction of the sharper component at 3706 cm^{-1} and a decrease of the intensity for the molecular adsorbed water. Upon evacuation at 573 K, only small features could be observed on Nb_2O_5, suggesting that most of the surface hydroxyl species have been removed.

The spectrum of $NbOPO_4$ presents a strong sharp band at 3667 cm^{-1} (see Fig. 12) which could be assigned to the OH stretching mode of surface phosphate or pyrophosphate species as reported by Armaroli et al. [21]. This band is also accompanied by a broad band around 3300 cm^{-1} and a band due to scissoring mode of adsorbed molecular water at 1616 cm^{-1}. The bands on $NbOPO_4$ exhibited much higher intensity than those on Nb_2O_5 (see the comparison in Fig. 11, inset), suggesting the presence of much larger amounts of surface hydroxyl and adsorbed water on $NbOPO_4$ than on Nb_2O_5. Moreover, upon outgassing at increasing temperature, the surface hydroxyl groups and adsorbed water on $NbOPO_4$ were much more stable than those on Nb_2O_5.

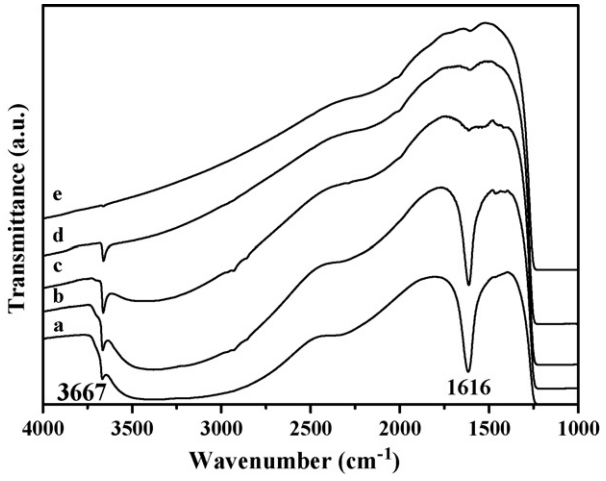

Fig. 12. FT-IR absorption bands of OH groups of the $NbOPO_4$ desorbed at different temperatures: (a) 300 K, (b) 423 K, (c) 573 K, (d) 673 K and (e) 773 K.

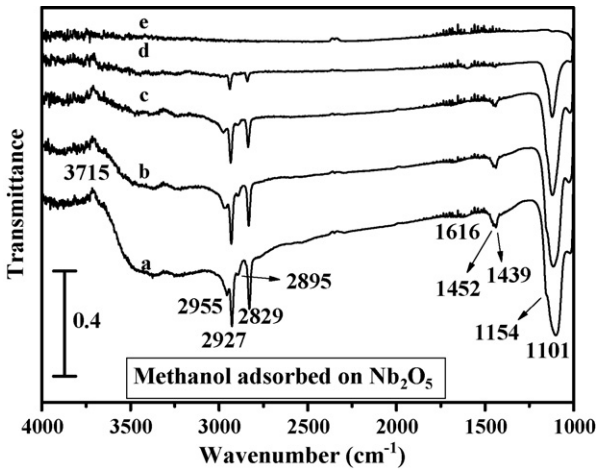

Fig. 13. FT-IR spectra for methanol adsorption and desorption on Nb_2O_5 catalyst at different temperatures: (a) 300 K, (b) 373 K, (c) 473 K, (d) 573 K and (e) 673 K.

3.4.3. Methanol adsorption FT-IR

The FT-IR spectra for methanol adsorbed on Nb_2O_5 and $NbOPO_4$ are shown in Figs. 13 and 14. On Nb_2O_5, which is shown in Fig. 13, a negative band appears at 3715 cm^{-1} due to the consumption of hydroxyl groups which were bonded with methanol, accompanied by a shoulder at 3400 cm^{-1} due to the hydrogen-bonded species. These features suggest the probable co-existence of molecularly adsorbed DME and CH_3O(a) (methoxy species) on the surface of Nb_2O_5. They are distinguishable by the characteristic symmetric ($\nu_s(CH_3)$) and antisymmetric ($\nu_{as}(CH_3)$) CH_3 stretching frequencies: 2829 and 2927 cm^{-1} for CH_3O(a), which are in good agreement with the results reported in the literature [38,39]. The band observed at 2955 cm^{-1} could be assigned to the $\nu_{as}(CH_3)$ vibration mode of molecularly adsorbed DME species formed by methanol dehydration [40]. The band at 2884 cm^{-1} is due to the C–H vibration of $2\delta(CH_3)$ bending mode. In the region of low wave number, the $\delta(CH_3)$ bending vibrations led to bands at 1452 and 1439 cm^{-1}

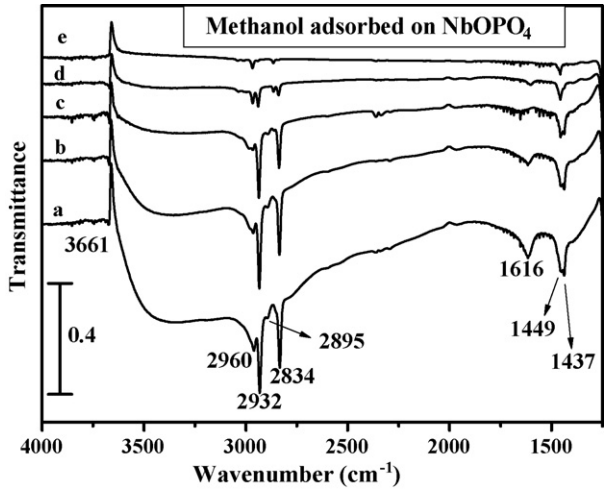

Fig. 14. FT-IR spectra for methanol adsorption and desorption on $NbOPO_4$ catalyst at different temperatures: (a) 300 K, (b) 373 K, (c) 473 K, (d) 573 K and (e) 673 K.

and the $\rho(CH_3)$ rocking mode is seen at 1154 cm^{-1}. In addition, a strong absorption band due to the C–O stretching mode of CH_3O(a) is visible at 1101 cm^{-1}, reflecting the presence of terminal methoxy adsorption species on the Nb_2O_5 surface. The band at 1616 cm^{-1} is due to the molecular adsorbed H_2O on Nb_2O_5, which might be produced via methanol dehydration on the surface. Below the 1000 cm^{-1} region, the bands could not be observed due to the strong background of CaF_2 windows.

The features of these peaks indicate that most of the methanol is dissociatively adsorbed to form methoxy species most likely acting as on-top adsorbed species, and a small amount of methoxy species might dehydrate to DME adsorbed on the surface of Nb_2O_5. Upon evacuation at elevated temperature, the intensities of all these bands decrease, indicating the removal of the surface species. Upon desorbing at 673 K for 0.5 h, all the bands disappeared or became extremely weak.

Similar band features could be observed on $NbOPO_4$ (see Fig. 14), although the bands below 1300 cm^{-1} could not be observed due to the strong background of $NbOPO_4$. The bands in the C–H stretching region on $NbOPO_4$ shifted to higher wave numbers than for Nb_2O_5. This probably suggests that the methoxy species adsorb more strongly on P atoms than on Nb atoms, since P exhibits a higher electronegativity value (2.2) than Nb (1.6) and attracts electrons more strongly, which results in weaker O–C bonding and enhanced C–H bonding in methoxy species. This observation is in agreement with the results of methanol TPD.

3.4.4. DME adsorption FT-IR

The adsorption of DME on alumina [41], H-ZSM-5 [42], ZrO_2 [43], etc. has been studied by FT-IR. Chen et al. reported that DME was molecularly adsorbed on alumina surface at low temperature (150 K) while it formed surface methoxy species when heated to temperatures higher than 250 K [41]. Feng and Yao suggested that the molecularly adsorbed DME was moderately dissociated on a dehydroxylated ZrO_2 surface, while it rapidly dissociated and no molecularly adsorbed DME could be observed on a fully hydroxylated ZrO_2 surface [43]. Fujino et al. suggested that DME molecules adsorbed on OH groups of H-ZSM-5 via hydrogen bonding irrespective of their acidity, and that the oxonium ions of DME were not produced on the studied surface [42].

The FT-IR results for DME adsorption on Nb_2O_5 and $NbOPO_4$ samples are shown in Figs. 15 and 16. In the case of $NbOPO_4$ (Fig. 16), the adsorption of DME caused an intense negative band at 3660 cm^{-1} which is surely due to the consumption of hydroxyl groups, suggesting DME adsorption on the hydroxyl groups of $NbOPO_4$. On Nb_2O_5, this negative band feature was not apparent, perhaps because of the low density of OH groups on Nb_2O_5 (see Fig. 11) after pretreatment by outgassing at 673 K.

In the wave number region corresponding to C–H stretching, the bands at 2954 ($\nu_{as}(CH_3)$), 2880 ($2\delta(CH_3)$) and 2841 ($\nu_s(CH_3)$) cm^{-1} were observed on Nb_2O_5 (Fig. 15). The bands in the δ(C–H) region are also detectable at 1458 and 1471 cm^{-1} due to $\delta(CH_3)$ bending vibration mode. The bands observed at 1252 and 1151 cm^{-1} are due to the $\gamma(CH_3)$ vibration mode

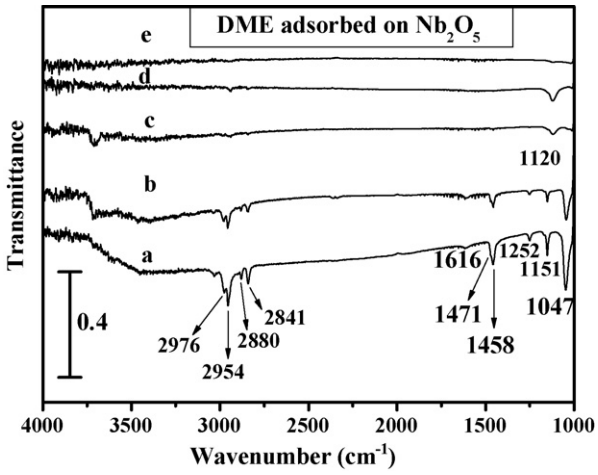

Fig. 15. FT-IR spectra for dimethyl ether adsorption and desorption on Nb_2O_5 catalyst at different temperatures: (a) 298 K, (b) 373 K, (c) 473 K, (d) 573 K and (e) 673 K.

and $\rho(CH_3)$ rocking mode, respectively. The band observed at 1047 cm^{-1} is due to the $\nu_{as}(CO)$ stretching mode [44]. Since these bands appeared at different wave numbers compared to the methoxy species formed by methanol adsorption, these band features can therefore be assigned to the C–H stretching modes of DME molecularly coordinated to a Lewis acid site on the surface, which is in agreement with the observations on ZrO_2 [40]. It is noted that there was also a weak band at 1616 cm^{-1} due to the scissoring vibration mode of molecular adsorbed water, which suggests that a small amount of DME was dissociatively adsorbed on the hydroxyl groups and thus formed H_2O. This might proceed by a mechanism in which DME molecules first react with an acidic proton to form a methanol molecule and a methyl group, and then the methanol thus formed can react with another Brønsted acid site to form $H_2O(g)$ and a second methyl group [45]. However, the bands for methoxy species could not be observed, suggesting that the amount of dissociatively adsorbed DME is very small.

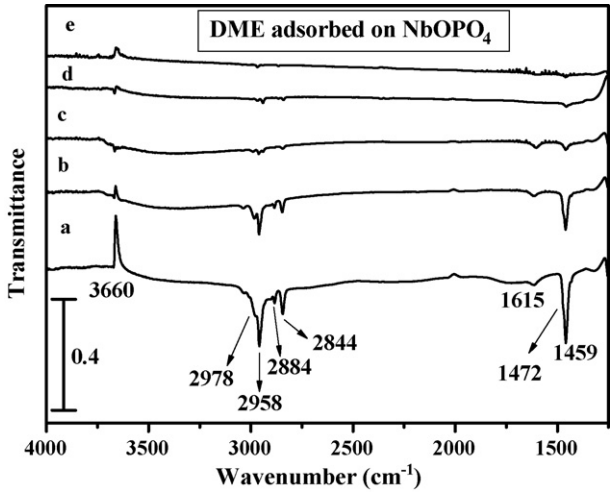

Fig. 16. FT-IR spectra for dimethyl ether adsorption and desorption on $NbOPO_4$ catalyst at different temperatures: (a) 298 K, (b) 373 K, (c) 473 K, (d) 573 K and (e) 673 K.

Similar bands were observed on $NbOPO_4$, indicating a similar adsorption situation. The bands for $NbOPO_4$ were shifted to higher wave numbers and exhibited higher intensities than on Nb_2O_5, implying the stronger interaction of adsorbed DME with $NbOPO_4$ than with Nb_2O_5.

Upon outgassing at 473 K, most of the bands disappeared on Nb_2O_5, while it seemed that some DME still remained on $NbOPO_4$, indicating again that DME is more strongly adsorbed on $NbOPO_4$ than on Nb_2O_5. A new band appearing at 1120 cm^{-1} upon outgassing at 473 K on Nb_2O_5 was not identified.

3.5. Reaction activity

The results for the dehydration of methanol to DME on Nb_2O_5 and $NbOPO_4$ catalysts are shown in Fig. 17. As a comparison, the results obtained on H-ZSM-5 and γ-Al_2O_3 catalysts in a previous work in our group are also given [9]. It can be seen that Nb_2O_5 and $NbOPO_4$ are much less active than H-ZSM-5, since the conversion of methanol on H-ZSM-5 reached the equilibrium at a temperature as low as 423 K [9], while the conversions on Nb_2O_5 and $NbOPO_4$ were only 0.8 and 3.2%, respectively. Below 553 K, Nb_2O_5 and $NbOPO_4$ were much more active than γ-Al_2O_3, and among them $NbOPO_4$ was more active than Nb_2O_5. For example, at 513 K, the conversions of methanol on γ-Al_2O_3, Nb_2O_5 and $NbOPO_4$ were 3.0, 12.8 and 28.5%, respectively. The activity of γ-Al_2O_3 increased quickly with increasing reaction temperature, while the activity of Nb_2O_5 and $NbOPO_4$ increased relatively slowly. The activity of $NbOPO_4$ reached a maximum at 593 K and then decreased with a further increase in temperature, which is due to the equilibrium limitation since the methanol dehydration reaction is exothermic. DME was the only organic product observed in the entire temperature range employed in this reaction, and no hydrocarbon by-products were detected on Nb_2O_5 and $NbOPO_4$. Moreover, no obvious deactivation of the Nb_2O_5 and $NbOPO_4$ catalysts could be observed during the time (12 h) over which the experiments were carried out. Moreover, very little coke was formed

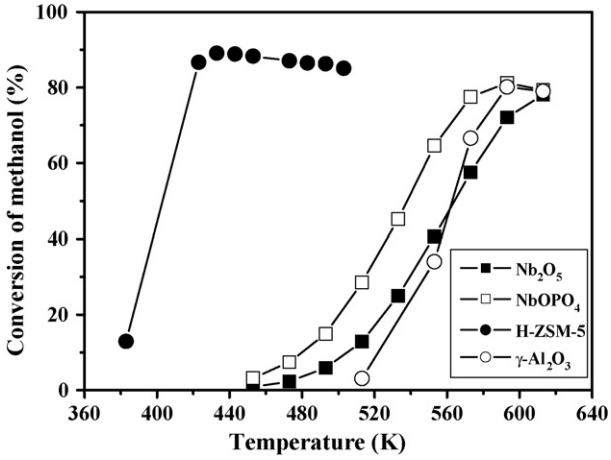

Fig. 17. Conversion of methanol at different temperatures over Nb_2O_5, $NbOPO_4$, H-ZSM-5 and γ-Al_2O_3 catalysts (the activities of H-ZSM-5 and γ-Al_2O_3 from the literature [9] are depicted as a comparison).

on Nb_2O_5 and $NbOPO_4$ after dehydration reaction. Comparatively, on H-ZSM-5, organic by-products were detected above 513 K, and the conversion of methanol decreased with the time on stream [9,11].

The activity of a suitable dehydration catalyst should be sufficient but not too high in order to prevent the formation of hydrocarbon products, which causes coke deposition and deactivation of the catalysts. The results suggest that even though the activities of Nb_2O_5 and $NbOPO_4$ in the methanol dehydration reaction were lower than that of H-ZSM-5, they showed 100% selectivity to DME and good stability. Thus, Nb_2O_5 and $NbOPO_4$ could be used as dehydration catalysts.

Note that the surface area of $NbOPO_4$ was much larger than that of Nb_2O_5, but the methanol dehydration activity of $NbOPO_4$ was only slightly higher than that of Nb_2O_5 especially at high temperature. It has been reported that the strength of Lewis acid sites on γ-Al_2O_3 was decreased upon the adsorption of water [46], and the partial pressure of water had a strong negative effect on the activity of γ-Al_2O_3 for the dehydration of methanol to DME [7]. Thus, the observed behavior could be ascribed to the stronger adsorption of H_2O and DME as well as the higher stability of methoxy species on $NbOPO_4$ than Nb_2O_5, as identified by the results of adsorption microcalorimetry and adsorption FT-IR experiments. In the methanol dehydration reaction, water, DME and methanol might comparatively adsorb on the acid sites of Nb_2O_5 and $NbOPO_4$. Since water and DME are products of the methanol dehydration reaction, strongly adsorbed water and DME might occupy some active acid sites on $NbOPO_4$ and therefore decrease the methanol dehydration activity, which is in agreement with the results reported by Bandiera and Naccache [47].

4. Conclusions

Amorphous Nb_2O_5 and $NbOPO_4$ samples were synthesized. The results of microcalorimetry and FT-IR for NH_3 adsorption showed that $NbOPO_4$ is much more acidic than Nb_2O_5 due to its high surface area, and that both Brønsted and Lewis acid sites are present on the surface of Nb_2O_5 and $NbOPO_4$. Water adsorption microcalorimetry results indicated that a small amount of water was strongly adsorbed on the Lewis acid sites of Nb_2O_5 and $NbOPO_4$, while most of the water was adsorbed by physical adsorption. The results of methanol adsorption microcalorimetry and methanol adsorption FT-IR suggest that methanol was mainly strongly dissociatively adsorbed on the surface of Nb_2O_5 and $NbOPO_4$ to form methoxy species as well as small amounts of DME and water molecularly adsorbed on the surface as products of the dehydration of methoxy species, as confirmed by the methanol TPD results. DME adsorption microcalorimetry and adsorption DME FT-IR showed that DME was mainly molecularly chemisorbed on Nb_2O_5 and $NbOPO_4$, while a small amount of DME could also be dissociatively adsorbed. $NbOPO_4$ exhibited stronger interaction with the probe molecules (NH_3, methanol, H_2O and DME) than Nb_2O_5. In the reaction of methanol dehydration, although the activities of Nb_2O_5 and $NbOPO_4$ were lower than that of H-ZSM-5, they exhibited 100% selectivity to the DME product and good stability of the activities, without coke formation.

Acknowledgements

We acknowledge the financial supports from the French Ministry of Education, the CNRS-France, NSFC (20673055) and MSTC (2004DFB02900 and 2005CB221400).

References

[1] T. Shikada, K. Fujimoto, M. Miyauchi, H. Tominaga, Appl. Catal. 7 (1983) 361–368.
[2] W.W. Kaeding, S.A. Butter, J. Catal. 61 (1980) 155–164.
[3] G.Y. Cai, Z.M. Liu, R.M. Shi, C.Q. He, L.X. Yang, C.L. Sun, Y.J. Chang, Appl. Catal. A 125 (1995) 29–38.
[4] T.H. Fleisch, A. Basu, M.J. Gradassi, J.G. Masin, Nat. Gas Conver. IV (1997) 117–125.
[5] J. Sehested, T. Mogelberg, T.J. Wallington, E.W. Kaiser, O.J. Nielsen, J. Phys. Chem. 100 (1996) 17218–17225.
[6] J.C. Woodhouse, US Patent 2,014,408 (1935).
[7] M.T. Xu, J.H. Lunsford, D.W. Goodman, A. Bhattacharyya, Appl. Catal. A 149 (1997) 289–301.
[8] J.H. Kim, M.J. Park, S.J. Kim, O.S. Joo, K.D. Jung, Appl. Catal. A 264 (2004) 37–41.
[9] Y.C. Fu, T. Hong, J.P. Chen, A. Auroux, J.Y. Shen, Thermochim. Acta 434 (2005) 22–26.
[10] W.K. Bell, C.D. Chang, US Patent 4,423,155 (1983).
[11] T. Takeguchi, K. Yanagisawa, T. Inui, M. Inoue, Appl. Catal. A 192 (2000) 201–209.
[12] J. Topp-Jorgensen, US Patent 4,536,485 (1985).
[13] G. Pagani, US Patent 4,098,809 (1978).
[14] G.C. Chinchen, J.R. Jennings, US Patent 4,863,894 (1989).
[15] V. Vishwanathan, K.W. Jun, J.W. Kim, H.S. Roh, Appl. Catal. A 276 (2004) 251–255.
[16] K. Tanabe, Mater. Chem. Phys. 17 (1987) 217–225.
[17] J.-M. Jehng, I.E. Wachs, Catal. Today 8 (1990) 37–55.
[18] K. Tanabe, Catal. Today 8 (1990) 1–11.
[19] I. Nowak, M. Ziolek, Chem. Rev. 99 (1999) 3603–3624.
[20] M. Ziolek, Catal. Today 78 (2003) 47–64.
[21] T. Armaroli, G. Busca, C. Carlini, M. Giuttari, A.M.R. Galletti, G. Sbrana, J. Mol. Catal. A 151 (2000) 233–243.
[22] S. Okazaki, M. Kurimata, T. Iizuka, K. Tanabe, Bull. Chem. Soc. Japan 60 (1987) 37–41.
[23] N.K. Mal, M. Fujiwara, Chem. Commun. (2002) 2702–2703.
[24] A. Auroux, Top. Catal. 4 (1997) 71–89.
[25] Q. Sun, A. Auroux, J. Shen, J. Catal. 244 (2006) 1–9.
[26] J. Cortes, M. Jensen, P. Araya, J. Chem. Soc., Faraday Trans. I 82 (1986) 1351–1355.
[27] Y.I. Tarasevich, V.E. Polyakov, A.A. Serdan, G.V. Lisichkin, Colloid J. 66 (2004) 592–597.
[28] H. Thamm, J. Chem. Soc., Faraday Trans. I 85 (1989) 1–9.
[29] B. Fubini, V. Bolis, A. Cavenago, E. Garrone, P. Ugliengo, Langmuir 9 (1993) 2712–2720.
[30] J. Janchen, J. van Wolput, W.J.M. Van Well, H. Stach, Thermochim. Acta 379 (2001) 213–225.
[31] V. Bolis, C. Busco, P. Ugliengo, J. Phys. Chem. B 110 (2006) 14849–14859.
[32] C.C. Lee, R.J. Gorte, W.E. Farneth, J. Phys. Chem. B 101 (1997) 3811–3817.
[33] V. Bolis, A. Cavenago, B. Fubini, Langmuir 13 (1997) 895–902.
[34] M.A. Natal-Santiago, J.A. Dumesic, J. Catal. 175 (1998) 252–268.
[35] G. Busca, P.F. Rossi, V. Lorenzelli, M. Benaissa, J. Travert, J.C. Lavalley, J. Phys. Chem. 89 (1985) 5433–5439.
[36] Y.W. Han, H. Zou, J.Y. Shen, W.J. Ji, Y. Chen, Chem. Lett. (1998) 1179–1180.

[37] J.C. Lavalley, J. Caillod, J. Chim. Phys. Phys. Chim. Biol. 77 (1980) 373–377.
[38] W.C. Wu, C.C. Chuang, J.L. Lin, J. Phys. Chem. B 104 (2000) 8719–8724.
[39] V. Boiadjiev, W.T. Tysoe, Chem. Mater. 10 (1998) 334–344.
[40] F. Ouyang, S. Yao, J. Phys. Chem. B 104 (2000) 11253–11257.
[41] J.G. Chen, P. Basu, T.H. Ballinger, J.T. Yates, Langmuir 5 (1989) 352–356.
[42] T. Fujino, M. Kashitani, J.N. Kondo, K. Domen, C. Hirose, M. Ishida, F. Goto, F. Wakabayashi, J. Phys. Chem. 100 (1996) 11649–11653.
[43] Q.Y. Feng, S.L. Yao, J. Phys. Chem. B 104 (2000) 11253–11257.
[44] E. Finocchio, M. Daturi, C. Binet, J.C. Lavalley, G. Blanchard, Catal. Today 52 (1999) 53–63.
[45] P. Cheung, A. Bhan, G.J. Sunley, E. Iglesia, Angew. Chem. Int. Ed. 45 (2006) 1617–1620.
[46] M. Li, J. Shen, J. Catal. 205 (2002) 248–258.
[47] J. Bandiera, C. Naccache, Appl. Catal. 69 (1991) 139–148.